

Beiträge aus der Elektrotechnik

Mengqi Cui

**Analysis and Design of Millimeter-wave Power
Amplification and Clock Generation in CMOS**



Dresden 2025

Bibliografische Information der Deutschen Nationalbibliothek
Die Deutsche Nationalbibliothek verzeichnet diese Publikation in der
Deutschen Nationalbibliografie; detaillierte bibliografische Daten sind im
Internet über <http://dnb.dnb.de> abrufbar.

Bibliographic Information published by the Deutsche Nationalbibliothek
The Deutsche Nationalbibliothek lists this publication in the Deutsche
Nationalbibliografie; detailed bibliographic data are available on the
Internet at <http://dnb.dnb.de>.

Zugl.: Dresden, Techn. Univ., Diss., 2025

Die vorliegende Arbeit stimmt mit dem Original der Dissertation
„Analysis and Design of Millimeter-wave Power Amplification and Clock
Generation in CMOS“ von Mengqi Cui überein.

© Jörg Vogt Verlag 2025
Alle Rechte vorbehalten. All rights reserved.

Gesetzt vom Autor

ISBN 978-3-95947-082-7

Jörg Vogt Verlag
Niederwaldstr. 36
01277 Dresden
Germany

Phone: +49-(0)351-31403921
Telefax: +49-(0)351-31403918
e-mail: info@vogtverlag.de
Internet : www.vogtverlag.de

Technische Universität Dresden

Analysis and Design of Millimeter-wave Power Amplification and Clock Generation in CMOS

Dipl.-Ing. Mengqi Cui

der Fakultät Elektrotechnik und Informationstechnik
der Technischen Universität Dresden
zur Erlangung des akademischen Grades

Doktoringenieur
(Dr.-Ing.)

vorgelegte Dissertation

Vorsitzender: Prof. Dr.-Ing. Dirk Plettemeier
Gutachter: Prof. Dr. sc. techn. Frank Ellinger
Prof. Dr.-Ing. Hermann Schumacher

Tag der Einreichung: 25. Juni 2024
Tag der Verteidigung: 7. Februar 2025

Acknowledgement

The implementation of design and characterization work carried out over the course of my PhD would not have been possible without the contributions of many people.

I would like to express my deepest gratitude to Prof. Frank Ellinger for his unwavering support, guidance, and invaluable insights throughout my doctoral journey. His mentorship has been instrumental in shaping my research and academic growth.

I am also indebted to Group Leaders Prof. Corrado Carta and Dr. Jens Wagner for providing a conducive research environment and fostering a culture of collaboration and innovation within our research group. Their leadership and encouragement have been pivotal in my development as a researcher.

I extend my sincere appreciation to Dr. Stefan Schumann for his technical expertise, assistance, and logistical support, which have been crucial for the successful completion of my experiments and projects. I would like to express my gratitude to several colleagues who engaged in numerous technical discussions with me on various topics, including circuit design and test fixture design. Some of them are Songhui Li, Xin Xu, Florian Protze, Paul Stärke, Jan Pliva, David Fritsche, Zoltan Tibenszky, Helmut Morath, and Manu Thayyil. I express sincere gratitude to Songhui Li for mentoring my Diplomarbeit and introducing me to the world of RFIC design.

I express my gratitude to Ms. Isaack, Ms. Muthmann, and Mr. Brandl, our Chair secretaries, as well as to our IT administrator, Mr. Bindrich, for their consistent support on numerous occasions.

To my parents, whose unwavering love, encouragement, and sacrifices have been the cornerstone of my academic journey, I owe you a debt of gratitude beyond words. Your belief in me has been my greatest motivation.

I would like to sincerely thank GlobalFoundries for generously providing the chip fabrication facility for the majority of the designs presented in this work. I am especially grateful to Mr. Ned Cahoon for initiating and facilitating the collaboration with TU Dresden, which has been instrumental to the success of our projects.

Last, but certainly not least, I am deeply grateful to my wife for her patience, understanding, and unwavering support throughout this challenging yet fulfilling endeavor. Your love and encouragement sustained me during the highs and lows of the PhD journey, and I am forever grateful.

Abstract

The demand for high-speed wireless communication systems has grown significantly in recent years. Millimeter-wave (mmWave) frequencies, especially the 60 GHz band, offer ample bandwidth for the demand. Simultaneously, integrating communication and sensing capabilities on a single platform has become a focus to increase the versatility and capability of modern RF front-ends. This integration optimizes hardware resources and fosters efficient wireless systems. While technologies like Silicon Germanium (SiGe) have been traditionally used for high-frequency RF front-ends, CMOS technology has gained prominence because of its unique advantages. CMOS offers superior integration capabilities with digital circuits, enabling energy-efficient systems with both communication and sensing functionalities on a single chip.

This thesis delves into cutting-edge mmWave RF front-end circuit design in a 22 nm FDSOI technology, particularly focused on 60 GHz applications and joint sensing and communication systems. Divided into two major parts, the thesis showcases significant advancements in circuit design efficiency and system integration.

The initial segment of the thesis is dedicated to the exploration of power amplifiers (PAs) operating at 60 GHz. A new operation class J/F which combines the benefit of both classes J and F is proposed. The J/F class revolutionizes PA efficiency by elongating the voltage swing by harnessing the second harmonic and refining the voltage and current waveforms via the third harmonic. To prove the concept of this theoretical framework, a 60 GHz PA was fabricated using the 22 nm FDSOI technology. Notably, this PA achieved a record-breaking Power Added Efficiency (PAE) of 42.3% while occupying a remarkably reduced active area. These accomplishments underscore the thesis's overarching goal of enhancing key performance metrics for power amplifiers, thereby addressing the demands of mmWave applications.

The second half of the thesis addresses low-power frequency synthesis at 30 GHz, incorporating a fractional-N synthesizer with dual charge pumps and a class D VCO which set the new record of Figure of Merit (FOM) among VCOs using the same 22 nm FDSOI technologies. The phase locked loop (PLL), with only 16 mW DC power, achieves comparable frequency chirp speed and RMS frequency error to the state-of-the-art PLLs with much higher consumption. In addition to its low power consumption, the proposed fractional-N PLL features a hybrid design, wherein the digital control circuits and sigma delta modulator (SDM) are imple-

mented in an FPGA, while other circuit components are integrated into a 22 nm chip. This hybrid architecture endows the PLL with exceptional flexibility, allowing seamless switching between different SDMs and control logic configurations. Also, this hybrid method makes it possible to utilize distinct semiconductor technologies to implement ultra-fast mmWave circuits and their corresponding logic circuits, leveraging the strengths of each technology. However, this approach introduces inherent additional delays between the SDM and frequency dividers, which may potentially disrupt the PLL's operation. This phenomenon is thoroughly studied in this thesis and a general solution is derived based on theoretical analysis.

In both communication and Frequency Modulated Continuous Wave (FMCW) radar systems, minimizing phase and amplitude errors in the local oscillator (LO) signal is critical for maintaining signal integrity, achieving accurate measurements, and ensuring reliable system operation. To ensure precise quadrature output at 60 GHz a novel super harmonic injection-locked oscillator (ILO) method is introduced, leveraging a unique phase accuracy mechanism based on a Marchand balun working the at second harmonic frequency. To prove the concept of the theoretical analysis, a super harmonic injection-locked oscillator (ILO) fabricated using the 22 nm FDSOI technology is proposed and characterized in the laboratory. This oscillator facilitates the generation of highly precise quadrature outputs with minimal phase and amplitude errors across its locking range.

By emphasizing the exceptional PAE achievement, the innovative working principle of the super harmonic ILO, and the effective resolution of PLL synchronization challenges, this thesis contributes significantly to advancing mmWave RF front-end circuit design, setting the stage for enhanced joint sensing and communication systems in the future.

Zusammenfassung

Die Nachfrage nach drahtlosen Hochgeschwindigkeitskommunikationssystemen ist in den letzten Jahren deutlich gestiegen. Millimeterwellenfrequenzen (mmWave), insbesondere das 60 GHz-Band, bieten ausreichend Bandbreite für diesen Bedarf. Gleichzeitig ist die Integration von Kommunikations- und Sensorfunktionen auf einer einzigen Plattform in den Fokus gerückt, um die Vielseitigkeit und Leistungsfähigkeit moderner HF-Frontends zu erhöhen. Diese Integration optimiert Hardwareressourcen und fördert effiziente drahtlose Systeme. Während Technologien wie Siliziumgermanium (SiGe) traditionell für Hochfrequenz-HF-Frontends verwendet wurden, hat die CMOS-Technologie aufgrund ihrer einzigartigen Vorteile an Bedeutung gewonnen. CMOS bietet überlegene Integrationsmöglichkeiten mit digitalen Schaltkreisen und ermöglicht energieeffiziente Systeme mit Kommunikations- und Sensorfunktionen auf einem einzigen Chip.

Diese Arbeit beschäftigt sich mit modernem mmWave Frontend Schaltungsdesign in einer 22 nm FDSOI Technologie, insbesondere für 60 GHz Anwendungen sowie der Entwicklung einer gemeinsamen Sensorik- und Kommunikationsplattform. In zwei Hauptteile unterteilt, präsentiert die Arbeit bedeutende Fortschritte in der Effizienz des Schaltungsdesigns und der Systemintegration.

Im ersten Teil der Arbeit werden 60 GHz Leistungsverstärker (PAs) untersucht. Es erfolgt die Einführung einer neuen Verstärkerklasse J/F, welche die Vorteile der Klassen J und F kombiniert. PAs aus der Klasse J/F weisen eine sehr hohe Effizienz auf. Um die entwickelte Theorie der neuen Verstärkerklasse zu verifizieren, wurde ein 60 GHz PA in einer 22 nm FDSOI Technologie gefertigt. Der PA-Prototyp hat eine Leistungssteigerungseffizienz von 42,3% erreicht. Zusätzlich fällt der aktive Flächenbedarf (von nur $0,0198 \text{ mm}^2$) extrem gering aus. Diese Errungenschaften unterstreichen das übergeordnete Ziel der Arbeit, die wesentlichen Leistungsmerkmale für PAs zu verbessern und damit den Anforderungen von mmWave-Anwendungen gerecht zu werden.

Die zweite Hälfte der Arbeit beschäftigt sich mit der Frequenzsynthese mit geringem Stromverbrauch bei 30 GHz, wobei ein Fractional-N-Synthesizer mit zwei Ladungspumpen und ein VCO der Klasse D verwendet werden, der den neuen Figure of Merit (FOM)-Rekord unter VCOs mit derselben 22 nm FDSOI-Technologie aufgestellt hat. Der Phasenregelkreis (PLL) erreicht mit nur 16 mW Verbrauch eine vergleichbare Frequenz Chirp Geschwindigkeit und RMS Frequenzfehler wie die PLLs auf dem neuesten Stand der Technik, bei viel höherem Verbrauch.

Zusätzlich zu seinem geringen Stromverbrauch zeichnet sich der vorgeschlagene Fractional-N PLL durch ein Hybriddesign aus, bei dem die digitalen Steuerschaltungen und der Sigma-Delta-Modulator (SDM) in einem FPGA implementiert sind, während andere Schaltungskomponenten in einen 22 nm Chip integriert sind. Diese Hybridarchitektur verleiht dem PLL eine außergewöhnliche Flexibilität und ermöglicht ein nahtloses Umschalten zwischen verschiedenen SDMs und Steuerlogikkonfigurationen. Außerdem ermöglicht diese Hybridmethode die Verwendung unterschiedlicher Halbleitertechnologien zur Implementierung ultraschneller mmWave Schaltungen und deren entsprechender Logikschaltungen, wobei die Stärken jeder Technologie genutzt werden. Dieser Ansatz führt jedoch inhärente zusätzliche Verzögerungen zwischen dem SDM und den Frequenzteilern ein, die den Betrieb des PLL möglicherweise stören können. Dieses Phänomen wird in dieser Arbeit gründlich untersucht und auf der Grundlage einer theoretischen Analyse eine allgemeine Lösung abgeleitet. Im Rahmen dieser Arbeit erfolgt eine fundierte Analyse dieses Phänomens. Abschließend wird eine umfassende Lösung erarbeitet.

Sowohl in Kommunikations- als auch in frequenzmodulierten Continuous Wave (FMCW) ist die Minimierung von Phasen- und Amplitudenfehlern im lokalen Oszillatorsignal (LO) entscheidend für die Aufrechterhaltung der Signalintegrität, das Erreichen genauer Messungen und die Gewährleistung eines zuverlässigen Systembetriebs. Um eine präzise Quadraturausgabe bei 60 GHz zu gewährleisten, wird eine neuartige Methode mit superharmonischem injektionsgekoppeltem Oszillator (ILO) eingeführt, die einen einzigartigen Phasengenauigkeitsmechanismus nutzt, der auf einem Marchand-Balun basiert, der bei der zweiten Harmonischenfrequenz arbeitet. Um das Konzept der theoretischen Analyse zu beweisen, wird ein superharmonischer injektionsgekoppelter Oszillator (ILO), der mithilfe der 22 nm FDSOI-Technologie hergestellt wurde, vorgeschlagen und im Labor charakterisiert. Dieser Oszillator ermöglicht die Erzeugung hochpräziser Quadraturausgaben mit minimalen Phasen- und Amplitudenfehlern über seinen gesamten Kopplungsbereich.

Das extrem hohe PAE des entwickelten Klasse J/F PAs zusammen mit dem neuartigen SILO und der effizienten und flexiblen PLL Synchronisation trägt maßgeblich zur Verbesserung des mmWave Schaltungsdesigns bei. Dadurch wird der Grundstein für verbesserte kompakt integrierte Sensorik und Kommunikationssysteme der Zukunft gelegt.

List of Abbreviations

AC Alternating Current.

BiCMOS Bipolar Complementary Metal-Oxide-Semiconductor.

CM Common Mode.

CMOS Complementary Metal-Oxide-Semiconductor.

DAC Digital-to-Analog Converter.

DAT Distributed-Active-Transformer.

DC Direct Current.

DDFS Direct Digital Frequency Synthesis.

DE Drain Efficiency.

DM Differential Mode.

EFM Error Feedback Machine.

EM Electromagnetic.

EuMA European Microwave Association.

EVM Error Vector Magnitude.

FDSOI Fully Depleted Silicon On Insulator.

FF Fast-Fast Corner.

FMCW Frequency Modulated Continuous Wave.

FOM Figure of Merit.

FPGA Field Programmable Gate Arrays.

FSM Finite-State Machine.

HDL Hardware Description Language.

I/Q In-phase and Quadrature-phase.

IEEE Institute of Electrical and Electronics Engineers.

ILFD Injection Locked Frequency Divider.

ISM-Band Industrial, Scientific and Medical Band.

LFSR Linear Feedback Shift Register.

LSB Least Significant Bit.

MASH Multi stAge noise SHaping.

mmWave Millimeter Wave.

MOSFET Metal-Oxide-Semiconductor Field-Effect Transistor.

MR Matching Ratio.

OM Output Matching Network.

OP-AMP Operational Amplifier.

PA Power Amplifier.

PAE Power Added Efficiency.

PD Phase Detector.

PFD Phase Frequency Detector.

PLL Phase Locked Loop.

PN Phase Noise.

PSD Power Spectral Density.

PVT Process, Voltage, Temperature.

QAM Quadrature Amplitude Modulation.

RF Radio Frequency.

SDM Sigma Delta Modulator.

SiGe Silicon Germanium.

SOI Silicon On Insulator.

List of Abbreviations

SS Slow-Slow Corner.

TL Transmission Line.

TT Typical-Typical Corner.

VCCS Voltage Controlled Current Source.

VCO Voltage Controlled Oscillator.

List of Symbols

- α Waveform selection parameter for class J amplifier.
- β Amplitude coefficient (from 0 to 1) corresponding to class B.
- δ Skin depth.
- η Power efficiency.
- I_D Drain current.
- I_{DDi} Diode current to model the drain current of a MOSFET.
- k Boltzmann constant.
- k Coupling factor of two coils.
- μ Permeability.
- ω Angular velocity.
- ω_n Natural frequency.
- ρ Conductivity.
- S_n Noise spectral power density.
- T Temperature in kelvin.
- V_D Drain voltage.
- V_{DD} Drain to drain voltage, supply voltage.
- V_{DS} Voltage between drain and source.
- V_{GS} Voltage between gate and source.
- ξ Damping factor.
- Z_L Load impedance.
- Z_S Source impedance.

Contents

Acknowledgement	I
Abstract	I
Abstract in German	IV
List of Abbreviations	VII
List of Symbols	XI
List of Figures	XV
List of Tables	XIX
1 Introduction	1
2 Millimeter Wave Power Amplifiers	5
2.1 Power amplifiers classes for millimeter wave frequencies	5
2.1.1 Load impedance control up to the second harmonic	8
2.1.2 Load impedance control of higher harmonics	12
2.2 Losses and matching networks	21
2.2.1 Loss mechanism	21
2.2.2 Loss analysis of matching networks	23
2.3 Power combining techniques	30
2.4 Design and implementation of a 60 GHz stacked PA	31
2.4.1 Circuit design	32
2.4.2 Measurement results	34
2.5 Design and implementation of a 60 GHz class J/F PA	38
2.5.1 Circuit design	38
2.5.2 Measurement results	42
3 Clock Generation at mm-Wave	47
3.1 System overview	47
3.2 Phase locked loop basics	51
3.2.1 Type I PLL	52
3.2.2 Type II PLL	53

3.2.3	Frequency synthesis and chirp generation	56
3.2.4	Major phase noise sources in type II PLL	57
3.3	Design of a 30 GHz Fractional-N PLL	61
3.3.1	System level simulation in integer-N mode	62
3.3.2	Sigma delta modulator for fractional-N PLL	67
3.3.3	System level design for fractional-N mode	80
3.3.4	Effect of the delay	81
3.3.5	Chirp generation with SDM	89
3.3.6	Design of PFD	93
3.3.7	Design of PFD and charge pumps	93
3.3.8	Design of the frequency dividers	98
3.3.9	Design of the class D VCO	103
3.3.10	PLL implementation and measurement	110
3.4	Design of a 60 GHz Super Harmonic Injection Locked Oscillator with Quadrature Outputs	116
3.4.1	Design of the ILFD	117
3.4.2	Design of the frequency doubler and balun	118
3.4.3	Measurement Results	119
4	Summary and Outlook	127
Bibliography		128
List of own publications		142

List of Figures

1.1	System diagram of a generic directed conversion RFFE	2
1.2	System diagram of a generic FMCW radar	2
2.1	Generic simple PA schematic	6
2.2	Transfer (a) and output (b) characteristics of the MOSFET model in Fig.2.1	7
2.3	Waveforms and load lines of class A, B and C amplifiers	9
2.4	Comparison of theoretical voltage waveform from class J* through B to J	11
2.5	Waveforms, voltage spectrum and load impedance of class B	12
2.6	Waveforms, voltage spectrum and load impedance of class J	13
2.7	Schematic of a class E amplifier	14
2.8	Simulated class E waveform with a C_P of 12 fF	15
2.9	Simulated class E waveform with a C_P of 24 fF	16
2.10	Simulated class E waveform with a C_P of 48 fF	16
2.11	Simulated load line and current spectrum of a normal class B and an over driven class B	17
2.12	Simulated waveforms of an over driven class B	19
2.13	Simulated waveforms, load line and voltage spectrum of a class F .	20
2.14	Simulated waveforms, load line and voltage spectrum of a class J/F	20
2.15	L-topology matching network	23
2.16	Matching network efficiency over MR and Q-factor	25
2.17	Matching network efficiency over MR	26
2.18	Matching network efficiency over MR	27
2.19	Equivalent circuit of an on chip transformer	27
2.20	Simplified transformer schematic	28
2.21	Z_1 and the ratio $\frac{ Z_1 }{Z_L}$	29
2.22	Power combining techniques	31
2.23	Schematic of the power amplifier [Cui+19] © 2019 EuMA	32
2.24	Simplified transistor layout [Cui+19] © 2019 EuMA	33
2.25	3D view of the one side of the pseudo-differential transistor array [Cui+19] © 2019 EuMA	34
2.26	3D view of the output balun [Cui+19] © 2019 EuMA	35
2.27	Chip photo [Cui+19] © 2019 EuMA	35

2.28	S-parameter measured and simulated [Cui+19] © 2019 EuMA	36
2.29	Power performance at [Cui+19] 55 GHz © 2019 EuMA	36
2.30	Power performance at [Cui+19] 61.25 GHz © 2019 EuMA	37
2.31	50 - 90 GHz silicon-based PAs [al23; CWE24] © 2024 IEEE	39
2.32	Schematic and layout sketch of the gain core [CWE24] © 2024 IEEE	39
2.33	Simulated waveforms of class B and J/F at $V_{DD} = 1$ V [CWE24] © 2024 IEEE	41
2.34	Design of the output matching network [CWE24] © 2024 IEEE	41
2.35	EM simulation results of the output matching network [CWE24] © 2024 IEEE	42
2.36	Chip photo [CWE24] © 2024 IEEE	43
2.37	Measured S-parameters [CWE24] © 2024 IEEE	43
2.38	Large signal measurement at 58 GHz [CWE24] © 2024 IEEE	44
2.39	Measured PAE and output power at peak PAE over frequency [CWE24] © 2024 IEEE	44
2.40	Measured large signal performance at 58 GHz over V_{DD} [CWE24] © 2024 IEEE	45
3.1	Block diagram of frequency synthesizer for millimeter wave frequency	48
3.2	Scatter plot of FOM and phase noise of state-of-the-art VCOs, data from [FA13; CWE23; CCE21; SBS16; TCE21; HMM19; MDW17]	50
3.3	Typical quality factors of inductors and varactors over frequency	51
3.4	Block diagram of a type I PLL	52
3.5	Transfer characteristics of mixer and XOR PDs	53
3.6	Block diagram of a type II PLL	54
3.7	PFD transfer characteristic, schematic and timing graph [Raz20]	54
3.8	Closed loop transfer function of noise from reference input	59
3.9	Closed loop noise transfer function of VCO	60
3.10	Closed loop noise transfer function of resister in the loop filter	61
3.11	Block diagram of proposed PLL for system level simulation in integer-N mode	63
3.12	Calculated transfer functions of the proposed PLL	64
3.13	Phase noise calculation and simulation results	66
3.14	Digital implementation of first order EFM s	68
3.15	PSD plot of 10-bit EFM s with input word of 256	69
3.16	PSD plot of 10-bit EFM s with input word of 666	70
3.17	Digital implementation of a MASH 1-1-1	72
3.18	Digital implementation of a MASH 1-1-1 with dithering at the third stage	73
3.19	Digital implementation of a MASH 1-1-1 with dithering at last two stages	73
3.20	Digital implementation of an HK-MASH 1-1-1	74

3.21 Simulated PSD of different MASH 1-1-1 at an input word of 256	74
3.22 Simulated PSD of different MASH 1-1-1 at an input word of 666	75
3.23 Transient simulation of different MASH 1-1-1 at an input word of 256	76
3.24 Simulated PSD of different order HK-MASH at an input word of 256	77
3.25 Simulated PSD 10-bit and 20-bit HK-MASH 1-1-1 and 20-bit at an input fraction of 0.25	78
3.26 Transient simulation of different order HK-MASH at an input word of 256	78
3.27 Calculated different orders of SDM phase noise in the PLL	80
3.28 Two cases of clock configuration	81
3.29 Block diagram of proposed PLL for system-level simulation	82
3.30 Locking process of different delay values using divider output as the clock for the MASH	82
3.31 Waveforms of the PLL at a delay of 5 ns in path (b)	84
3.32 Waveforms of the PLL at a delay of 16 ns in path (b)	85
3.33 Locking process of different delay value using reference as the clock for the MASH	86
3.34 Waveforms of the PLL at a delay of 1.6 ns in path (a)	88
3.35 Delay time vs locking ability in path (a) and (b)	89
3.36 Chirp simulation with 2 nd order HK-MASH and a step size of 800	91
3.37 Chirp frequency error simulation with HK-MASH from 2 nd to 4 th order and a step size of 800 and a loop bandwidth of 400 kHz	92
3.38 Block diagram of the PFD/CP	94
3.39 Schematic of the charge pump without OP-AMP	95
3.40 DC simulation results of the charge pump CP1	95
3.41 Schematic of the charge pump with OP-AMP	96
3.42 DC simulation results of the charge pump CP2	97
3.43 Transient simulation results of the charge pump CP2	97
3.44 Schematic of the PFD	98
3.45 Transient simulation of the PFD	99
3.46 Block diagram of the divider chain	100
3.47 Schematic of the TSPC divider	101
3.48 Transient simulation of two stages of cascaded TSPC dividers for upper input frequency limit	102
3.49 Transient simulation of two stages of cascaded TSPC dividers for lower input frequency limit	102
3.50 Gate level schematic of the programmable divider	103
3.51 Transient simulation of two stages of cascaded programmable dividers	104
3.52 Schematic of the VCO [CWE23] © 2023 IEEE	105
3.53 Simulated tank impedance [CWE23] © 2023 IEEE	106
3.54 Simulated voltage and current waveform [CWE23] © 2023 IEEE .	106

3.55	Measured and simulated phase noise [CWE23] © 2023 IEEE	107
3.56	Chip photo of the VCO [CWE23] © 2023 IEEE	108
3.57	Measured and simulated tuning range [CWE23] © 2023 IEEE	108
3.58	Measured phase noise over tuning voltage [CWE23] © 2023 IEEE	108
3.59	Block diagram of the implementation of the PLL	110
3.60	Chip photo of the PLL	111
3.61	Phase noise measurement of the PLL	111
3.62	Chirp measurement and frequency error calculation	113
3.63	Some more chirp measurements	113
3.64	Block diagram of the QILO	117
3.65	Schematic of the ILFD	118
3.66	DC power consumption of different blocks	119
3.67	Chip photo	120
3.68	Picture of 120 GHz balun and its electromagnetic (EM) simulation results.	120
3.69	Measured S-parameters	121
3.70	Chirp measurement	122
3.71	Phase noise measurement	123
3.72	Measured locking range and S_{21} at a port power of 0 dBm at different V_{tune}	123

List of Tables

1.1	Circuit block requirements for different front-ends at millimeter wave frequency	3
2.1	Class E calculation at 60 GHz	15
2.2	Load impedances for class AB and J/F in large signal simulations [CWE24] © 2024 IEEE	40
2.3	State-of-the-art PAs around 60 GHz [CWE24] © 2024 IEEE . . .	46
3.1	Phase noise calculation for 60 GHz clock generation	49
3.2	Noise sources of a type II PLL	62
3.3	Design values of the 3 rd loop filter	64
3.4	Native output states of a MASH 1-1-1 and the corresponding division ratio	71
3.5	Modified a MASH 1-1-1 and the corresponding division ratio . . .	71
3.6	Design values of the 3 rd order loop filter	90
3.7	State-of-the-Art VCOs around 30 GHz [CWE23] © 2023 IEEE . .	109
3.8	Comparison with other mm-wave PLLs	114
3.9	Comparison with other mm-wave quadrature phase generation . .	124

1 Introduction

In an era marked by the relentless pursuit of higher data rates and the boom of various intelligent applications that require localization and range detection, millimeter-wave frequencies have emerged as the frontier of innovation, with their substantial bandwidth and potential for ultra-high data rates and fine resolutions, holds the promise of transforming numerous industries, including telecommunications, healthcare, automotive, and beyond.

The 60 GHz band within the millimeter-wave frequencies (30 GHz to 300 GHz) has garnered significant interest. Operating at this frequency allows for extremely compact radio frequency front-end (RFFE) sizes, enabling the integration of multiple RFFEs into a single handheld or wearable device. Despite the relatively strong absorption by the atmosphere, this characteristic becomes advantageous for communication purposes. It helps in reducing interferences over distances compared to other frequencies, amplifying its suitability for various applications. Moreover, even without employing the most advanced CMOS technologies, the 60 GHz frequency still provides a considerable amount of gain, making it a feasible choice for consumer electronics. Consequently, it has been adopted by several WiFi standards like 802.11ad and ay.

Thanks to the generous bandwidth available in the 60 GHz band compared to the congested sub-6 GHz bands, it is not always necessary to employ high-level modulation techniques such as 1024 quadrature amplitude modulation (QAM) with a high peak-to-average-power ratio (PAPR) to achieve the desired data rate. For instance, the latest WiFi-7 802.11be standard [KLA20] allows for a maximum channel bandwidth of 320 MHz and 4096-QAM, theoretically providing a data rate of 3.84 Gbps. However, such high-order modulation results in minimal separation between adjacent states, imposing stringent requirements on the linearity and noise performance of transceivers, typically leading to high power consumption.

In contrast, operating at 60 GHz, even the older 802.11ad WiFi standard from 2012, without channel bonding, offers a single channel bandwidth of 2.16 GHz. By employing robust QPSK (4-QAM) modulation, the theoretical data rate can reach 4.32 Gbps. Moreover, in both scenarios, the data rate can be further enhanced through faster-than-Nyquist (FTN) signaling [ARÖ13]. Since the basic modulation scheme without amplitude modulation imposes no linearity requirements, transmitters, particularly power amplifiers (PAs), can operate at their peak efficiency points, akin to radar PAs. Given that PAs are typically the most power-hungry components in modern wireless transceivers, their power consumption and

efficiency heavily influence the overall system performance.

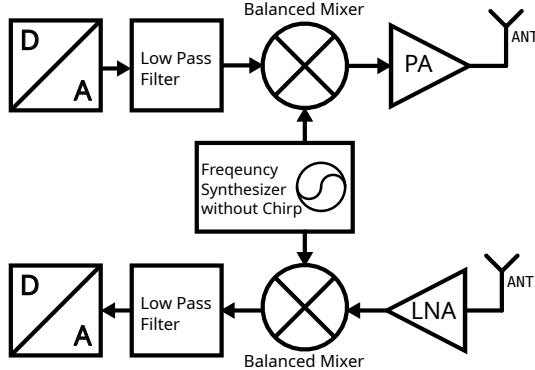


Figure 1.1: System diagram of a generic directed conversion RFFE

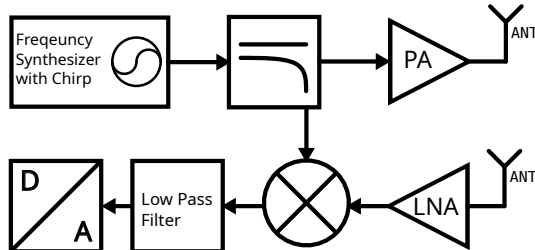


Figure 1.2: System diagram of a generic FMCW radar

The FMCW (Frequency Modulated Continuous Wave) radar, being one of the most popular radar topologies, has garnered increased attention in recent decades. This heightened interest stems not only from the enhanced resolutions offered by millimeter-wave frequencies but also from the similarity between an FMCW front-end and the widely used direct conversion RFFE. This similarity makes the integration of sensing and communication in a single front-end an intriguing option.

Figures 1.1 and 1.2 illustrate the generic block diagrams of a zero-IF (Intermediate Frequency)/direct conversion RFFE and an FMCW radar, respectively. The receiver paths in both block diagrams are highly similar. However, a significant difference lies in the transmitter path due to chirp generation typically being handled by the frequency synthesizer. Compared to the method of fixing

the LO (Local Oscillator) frequency and sweeping the baseband frequency using the analog-to-digital converter (DAC), frequency synthesizers offer superior power and cost efficiency over high-speed DACs. Furthermore, when generating a frequency chirp by sweeping the baseband frequency, the output of the up-mixer must be redirected to the LO input of the down-mixer to ensure synchronization of the LO frequency with the transmitted signal. This additional step increases system complexities.

Most direct conversion RFFEs utilize single- or double-balanced up-mixers to minimize LO signal leakage and typically do not require frequency chirp generation from their frequency synthesizer. In contrast, FMCW radars necessitate both frequency chirp generation and transmission of the LO signal. Table 1.1 outlines the circuit block requirements for different front-ends at millimeter-wave frequencies.

	zero-IF	FMCW	Joint
PA linearity	modulation dependent	no	modulation dependent
Up – mixer	balanced	no up-mixer	switchable between balanced and unbalanced
Down – mixer	balanced	balanced	balanced
Baseband BW	GHz range	MHz range	GHz range
Frequency synthesizer	chirp is not needed	chirp	chirp

Table 1.1: Circuit block requirements for different front-ends at millimeter wave frequency

Over the last decades, complementary metal-oxide semiconductor(CMOS) technology has been the major technology in volume production for almost all kinds of circuits. The continuous scaling of CMOS technologies boost the unity current gain frequency (f_t) and maximum oscillation frequency (f_{max}) to over 350 GHz, where the f_t is a commonly used metric for analog/mixed signal circuits and f_{max} is a more relevant metric for RF and millimeter-wave frequencies [Ven]. Unlike f_t , which is more a function of process technology, the f_{max} is strongly dependent on layouts. The transistors used in real designs, especially in PAs, have much more fingers and total width than the transistors used for benchmarking the technology. As a result, even in one of the most advanced CMOS technologies, the transistors in real designs together with the necessary layout for interconnects usually have f_{max} about 20 % to 30 % lower than the benchmarks. Silicon germanium (SiGe) technologies also have the same issue. Therefore, most PAs at 60 GHz need to operate at class-A or class-AB to obtain enough gain. The peak power added

efficiency (PAE) and drain efficiency (DE) are usually lower than 30 % [ala].

Apart from PAs, local oscillator (LO) signal generation or clock generation at millimeter-wave frequencies is also more demanding than it is at lower frequencies. In particular, voltage-controlled oscillators (VCOs) suffer from higher energy consumption and worse phase noise performance due to lower intrinsic gain offered by transistors and the limited quality factor of the tanks at millimeter-wave frequencies. In-phase and quadrature-phase (IQ) generation at sub-6 GHz can be generated easily with poly-phase filters or ring oscillators. While at millimeter-wave frequencies these approaches are not practical because of the high power losses and phase noise penalty of ring oscillators.

This thesis addresses two primary challenges in millimeter-wave RFFE for joint sensing and communication: power-efficient PAs and frequency synthesizers. Chapter 2 will begin with an overview of amplifier classes, including current-mode and switch-mode amplifiers. It will then delve into the principles of efficiency enhancement in power amplifiers, with a specific focus on millimeter-wave frequencies. Following the theoretical discussion, Chapter 2 will present the design and implementation of two power amplifiers operating at 60 GHz. Firstly, it will cover the design process of a class-AB stacked power amplifier, considering factors such as gate capacitance and phase alignment. This will be followed by the design and implementation of a higher-efficiency class-J/F PA.

Chapter 3 begins with an introduction and discussion on the basics of Type I and II PLLs. The modeling of all PLL components is then introduced and analyzed, including system-level simulation and a discussion on incorporating a sigma-delta modulator (SDM) with the PLL. Following the theoretical discussion, the chapter presents the design and implementation of a 30 GHz PLL with accurate chirp generation. Towards the end of this chapter, a super-harmonic injection-locked oscillator will be introduced to generate quadrature output over a wide bandwidth at 60 GHz .

In Chapter 4, a summary of the research findings in this thesis will be presented, along with recommendations for further work.